

# Many-body theory of positronium-atom interactions

D. G. Green,<sup>\*</sup> A. R. Swann,<sup>†</sup> and G. F. Gribakin<sup>‡</sup>

Centre for Theoretical Atomic, Molecular, and Optical Physics, School of Mathematics and Physics,  
Queen's University Belfast, Belfast BT7 1NN, Northern Ireland, United Kingdom

(Dated: December 14, 2024)

The many-body theory of positronium-atom interaction has been developed. As first applications, we calculate the elastic scattering and momentum-transfer cross sections and the pickoff annihilation rate  ${}^1Z_{\text{eff}}$  for positronium collisions with He and Ne. The cross section for He is in agreement with previous coupled-state calculation, and the momentum-transfer cross section for Ne agrees with available experimental data.  ${}^1Z_{\text{eff}}$  is calculated to be 0.13 and 0.26 for He and Ne, respectively, in excellent agreement with the measured values.

Positronium (Ps) is a light and simple “atom” consisting of an electron and its antiparticle, the positron. Recent experiments on Ps scattering on noble-gas atoms revealed some unexpected trends, e.g., that the scattering cross section becomes very small at low Ps energies [1]. Overall, there is a large uncertainty in the existing Ps-atom scattering data, and the best previous calculations [2–10] of the rate of *pickoff* annihilation on noble gases (where the positron from Ps annihilates with an atomic electron) underestimate the experimental data [11, 12] by as much as a factor of ten.

The theoretical description of Ps-atom interactions is challenging because of the composite nature of both the target and projectile and a significant cancellation between the repulsive static Ps-atom interaction and van-der-Waals-type attraction. Accurate calculations must account for dynamical distortion of both objects during the collision, which has only been achieved for simple targets, e.g., hydrogen and helium [13]. Calculations of the pickoff annihilation rate require account of important short-range electron-positron interactions; these are described via corrections to the annihilation vertex [14–16] and have been neglected in all previous calculations.

Many-body theory (MBT) provides a powerful, natural, and systematic method of accounting for the distortion of both objects and the electron-positron correlation effects. It has provided much success in describing low-energy electron [17–23] and positron [15, 16, 24–28] interaction with atoms, with scattering cross sections, annihilation rates, and  $\gamma$  spectra all found to be in excellent agreement with experiment.

In this Letter we combine the MBT description of electron-atom and positron-atom interactions to describe Ps interacting with a many-electron atom, including the important effect of screening of the electron-positron Coulomb interaction by the atom. As first applications of the theory, we calculate phase shifts, elastic-scattering and momentum-transfer cross sections, and the pickoff annihilation rate  ${}^1Z_{\text{eff}}$  for Ps on He and Ne. The cross sections are found to be in agreement with previous coupled-state [13] and model van der Waals [10] calculations. By accounting for electron-positron correlation corrections to the annihilation vertex, we obtain values of  ${}^1Z_{\text{eff}}$  in excellent agreement with experiment [11]. Atomic units (a.u.) are used throughout.

*MBT of electron- and positron-atom interactions.*—MBT describes an electron or positron in the field of a  $Z$ -electron atom via the Dyson equation for the (quasiparticle) wave func-

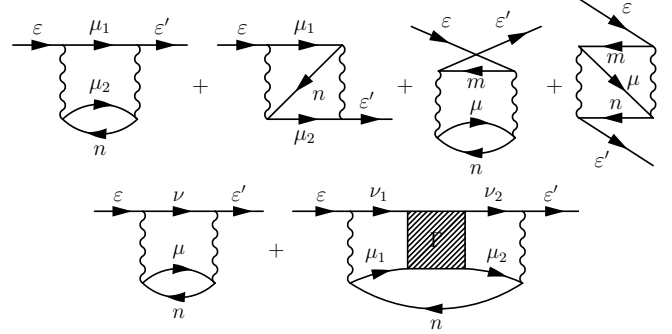


FIG. 1. The main contributions to the self-energy of the electron (top line) and positron (bottom line) in the field of the atom. Lines labeled  $\varepsilon$  represent the electron or positron HF wave function. Lines labeled  $\nu$  ( $\mu$ ) represent positron (excited electron) states, which are summed over. Lines labeled  $n$  and  $m$  represent holes in the atomic ground state. Wavy lines represent Coulomb interactions. The shaded  $\Gamma$  block represents the sum of the electron-positron ladder-diagram series [15, 26], which accounts for virtual Ps formation.

tion  $\psi_\varepsilon$  [29, 30]:

$$(\hat{H}_0^\pm + \hat{\Sigma}_\varepsilon^\pm)\psi_\varepsilon(\mathbf{r}) = \varepsilon\psi_\varepsilon(\mathbf{r}). \quad (1)$$

Here  $\hat{H}_0^\pm$  is the zeroth-order Hamiltonian, e.g., that of the electron (–) or positron (+) in the field of the Hartree-Fock (HF) ground-state atom, and  $\hat{\Sigma}_\varepsilon^\pm$  is the nonlocal, energy-dependent correlation potential [31], given by the irreducible self-energy of the electron or positron in the field of the target atom. Equation (1) can be solved separately for each partial wave, with the wave function of central-field form  $\psi_\varepsilon(\mathbf{r}) = r^{-1}\tilde{P}_{\varepsilon\ell}(r)Y_{\ell m}(\hat{\mathbf{r}})$ , where  $Y_{\ell m}$  is a spherical harmonic for the electron or positron with angular momentum  $\ell$  and projection  $m$ . Rather than computing the self-energy  $\Sigma_{E\ell}^\pm(\mathbf{r}, \mathbf{r}')$  in the coordinate basis, it is more convenient to work with its matrix elements  $\langle \varepsilon' | \Sigma_{E\ell}^\pm | \varepsilon \rangle$  in the HF basis  $\{\varphi_\varepsilon\}$ , where  $H_0\varphi_\varepsilon = \varepsilon\varphi_\varepsilon$ ,  $\varphi_\varepsilon(\mathbf{r}) = r^{-1}P_{\varepsilon\ell}(r)Y_{\ell m}(\hat{\mathbf{r}})$ , and  $\langle \varepsilon' | \Sigma_{E\ell}^\pm | \varepsilon \rangle = \iint P_{\varepsilon'\ell}(r')\Sigma_{E\ell}^\pm(r, r')P_{\varepsilon\ell}(r) dr dr'$ , with  $\Sigma_{E\ell}^\pm$  the self-energy for partial wave  $\ell$ . Using the completeness of the basis, it can be expressed as

$$\Sigma_{E\ell}^\pm(r, r') = \sum_{\varepsilon, \varepsilon'} P_{\varepsilon'\ell}(r') \langle \varepsilon' | \Sigma_{E\ell}^\pm | \varepsilon \rangle P_{\varepsilon\ell}(r). \quad (2)$$

Figure 1 shows the main contributions to the matrix elements of  $\Sigma_{E\ell}^-$  (top) and  $\Sigma_{E\ell}^+$  (bottom). For the electron, the

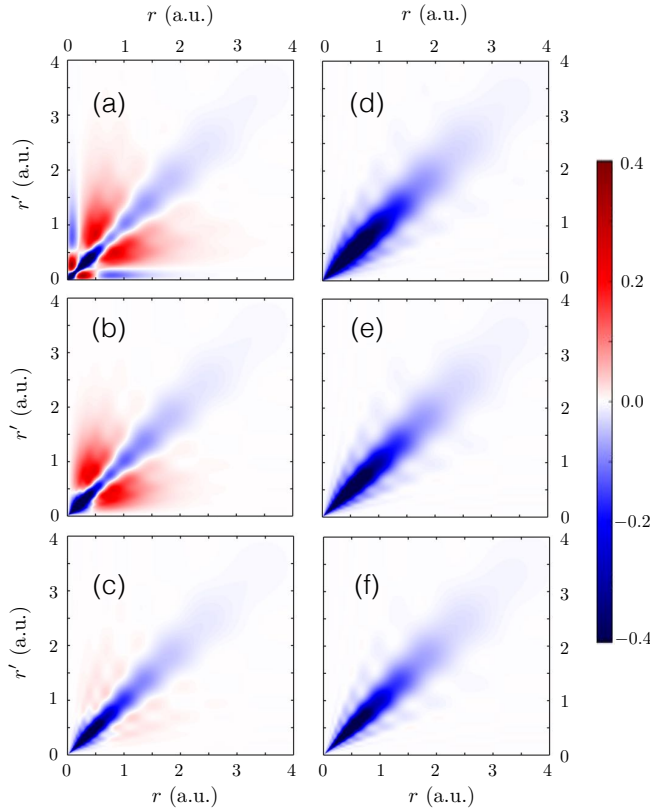


FIG. 2. Self-energy  $\Sigma_{E\ell}^{\pm}(r, r')$  at  $E = 0$  for electron (a)–(c) and positron (d)–(f) in the field of Ne, for  $\ell = 0, 1$ , and  $2$ , respectively.

first diagram accounts for the attractive long-range polarization potential  $-\alpha_d/2r^4$ , where  $\alpha_d$  is the dipole polarizability of the atom. The other three diagrams contribute only at short range. Accounting for these second-order diagrams provides a good description of the electron–noble-gas-atom system [21–23, 32][33]. For the positron, the first diagram gives rise to a similar long-range polarization potential as for the electron. In addition to this diagram, there is an important contribution of virtual Ps formation [15, 16, 25, 26]. It is described by the second diagram in which where the  $\Gamma$  block represents the sum of the infinite electron-positron ladder-diagram series [15]. We calculate the self-energies as described in Ref. [15], using a  $B$ -spline basis with 40 splines of order 6 defined over an exponential knot sequence, discretizing the continuum by confining the system in a spherical cavity of radius 30 a.u. This knot sequence provides an efficient spanning of the continuum and rapid convergence in the sums over intermediate states.

The correlation potential described by the self-energy is essentially nonlocal. It is also quite different for the electron and positron, and for different electron and positron partial waves. Figure 2 shows  $\Sigma_{E\ell}^{\pm}(r, r')$  for the  $s$ ,  $p$ , and  $d$  waves in Ne, calculated at  $E = 0$ . The main feature is a “valley” along the diagonal  $r = r'$ , whose width characterizes the degree to which  $\Sigma^{\pm}$  is nonlocal. The main contribution to electron- and positron-atom attraction comes from  $r \gtrsim 1$  a.u. (i.e., outside

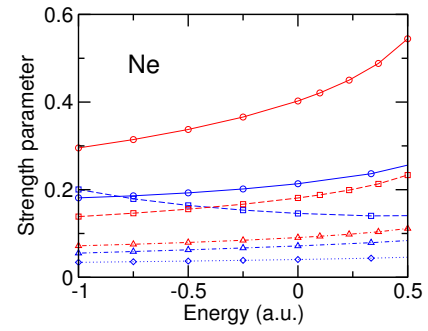


FIG. 3. The dimensionless strength parameter  $S_{E\ell}^{\pm}$  of the correlation potentials for the electron (blue) and positron (red) in the field of Ne, as a function of energy  $E$ , for  $\ell = 0$  (circles),  $\ell = 1$  (squares),  $\ell = 2$  (triangles), and  $\ell = 3$  (diamonds). Lines are interpolants.

the atom). Here the minimum in  $\Sigma_{E\ell}^{\pm}(r, r')$  is deeper for the positron than the electron, meaning stronger attraction for the positron. As a consequence of the Pauli principle, the correlation potential for the electron is quite different for different partial waves. It is also significantly more nonlocal than that of the positron, with prominent repulsive contributions for the  $s$  and  $p$  waves. These features are due to the contribution of the second, exchange diagram to  $\Sigma_{E\ell}^{-}(r, r')$ . For both the electron and positron,  $\Sigma_{E\ell}^{\pm}$  becomes increasingly local for larger  $\ell$ .

The electron and positron correlation potentials are also energy dependent. This dependence can be analyzed using the dimensionless strength parameter  $S_{E\ell}^{\pm} = -\sum_{\varepsilon} \langle \varepsilon | \Sigma_{E\ell}^{\pm} | \varepsilon \rangle / \varepsilon$  [34] [35]. Figure 3 shows  $S_{E\ell}^{\pm}$  for Ne, as a function of energy for electron and positron  $s$ ,  $p$ ,  $d$ , and (for the electron)  $f$  waves. It confirms that the correlation potential is stronger for the positron. It also shows that its energy dependence is relatively weak on the energy scale of Ps (0.25 a.u.). This is important for the description of Ps-atom interaction, as it allows us to use  $\Sigma_{E\ell}^{\pm}(r, r')$  calculated for a fixed energy ( $E = 0$ ).

*MBT of Ps-atom interactions.*— The wave function  $\Psi$  of Ps in the field of the atom satisfies the two-particle Dyson equation (TPDE):

$$(\hat{H}_0^- + \hat{\Sigma}_{\varepsilon^-}^- + \hat{H}_0^+ + \hat{\Sigma}_{\varepsilon^+}^+ + V + \delta V_E)\Psi = E\Psi, \quad (3)$$

where  $V$  is the electron-positron Coulomb interaction and  $\delta V_E$  is the screening correction due to polarization of the atom. The diagrams for  $\delta V_E$  are shown in Fig. 4. Diagram (b) describes screening of  $V$  by the atomic electrons. They are essential for cancelling the long-range  $r^{-4}$  polarization attraction and making the long-range Ps-atom interaction of the required  $R^{-6}$  van der Waals form, where  $R$  is the distance between the Ps center of mass and the atom. The exchange corrections (c) and (d) are typically much smaller. They also partly cancel each other due to their opposite signs, and can be neglected.

The Ps eigenstates with angular momentum  $J$  and parity  $\Pi$ , are constructed from the single-particle Dyson states [36]

$$\Psi_{J\Pi}(\mathbf{r}_e, \mathbf{r}_p) = \sum_{\mu, \nu} C_{\mu\nu}^{J\Pi} \psi_{\mu}(\mathbf{r}_e) \psi_{\nu}(\mathbf{r}_p), \quad (4)$$

with coefficients  $C_{\mu\nu}^{J^\Pi}$ . Solution of Eq. (3) reduces to the matrix eigenvalue problem  $\mathbf{HC} = \mathbf{EC}$  for the Hamiltonian matrix

$$\langle \nu' \mu' | H | \mu \nu \rangle = (\varepsilon_\mu + \varepsilon_\nu) \delta_{\mu' \mu} \delta_{\nu' \nu} + \langle \nu' \mu' | V + \delta V_E | \mu \nu \rangle, (5)$$

where  $\mathbf{C}$  is the vector of coefficients. We choose  $J^\Pi = 0^+$ ,  $1^-$ , and  $2^+$  to investigate Ps  $S$ -,  $P$ -, and  $D$ -wave scattering, respectively. To ensure accurate description of Ps states by Eq. (4), we confine the electron and positron states to a cavity of radius  $R_c = 10$ – $16$  a.u. [36]. To accurately represent the positive-energy “continuum” in the cavity we use a second  $B$ -spline basis of 60 splines of order 9 defined over a quadratic-linear knot sequence [10]. Given the decrease of  $\Sigma_{E\ell}^\pm$  with the single-particle angular momenta  $\ell$  (see Figs. 2 and 3), we find that it is sufficient to use Dyson states in Eq. (4) for  $\ell \leq 3$  and use HF states for higher  $\ell$ . We exploit the weak energy dependence of  $\Sigma_{E\ell}^\pm$  and  $\delta V_E$  by evaluating them at  $E = 0$  [37]. Calculations are performed with different numbers of radial and angular states included in Eq. (4), up to  $n_{\max} = 20$  and  $\ell_{\max} = 20$ . The Ps eigenenergies are found and extrapolated to  $n_{\max} \rightarrow \infty$  and  $\ell_{\max} \rightarrow \infty$  as described in Ref. [36].

*Ps scattering on He and Ne.*—As a first application, we calculate the phase shifts and cross sections for Ps scattering on He and Ne. The phase shifts are determined from the Ps energy eigenvalues using the boundary condition on the Ps center-of-mass motion at the cavity wall, as described in Ref. [10]. Calculations were performed using cavity radii of 10, 12, 14, and 16 a.u. Effective-range-type fits were used to interpolate the  $S$ ,  $P$ , and  $D$  phase shifts calculated at the discrete values of the Ps center-of-mass momentum  $K$ . These fits were used to determine the scattering length and the partial contributions to the elastic and momentum-transfer cross sections.

The total and partial elastic scattering cross sections are shown in Fig. 5 (a) and (b) for He and Ne, respectively. For He, the  $S$ -wave contribution dominates across the range of momenta considered, but for Ne, the  $P$ -wave contribution becomes comparable at  $K \approx 1$  a.u. For He, the total elastic cross section is in good agreement with the 9-Ps-9-He coupled-state calculation of Walters *et al.* [13] and is close to the calculation in which a model van-der-Waals potential was added to the frozen-target Ps-atom interaction (FT+vdW) [10] for  $K \gtrsim 0.5$  a.u. [44]. Our scattering length of 1.70 a.u. compares well with the value of 1.6 a.u. obtained by Walters *et al.*

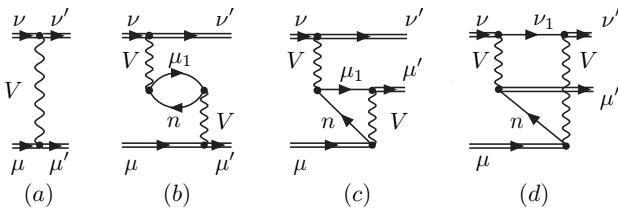


FIG. 4. The main contributions to the electron-positron interaction in Ps: (a) the bare Coulomb interaction  $V$ ; (b)–(d), screening  $\delta V_E$  with exchange contributions (and mirror images). Double lines labeled  $\nu$  ( $\mu$ ) represent positron (electron) Dyson states in the field of the atom.

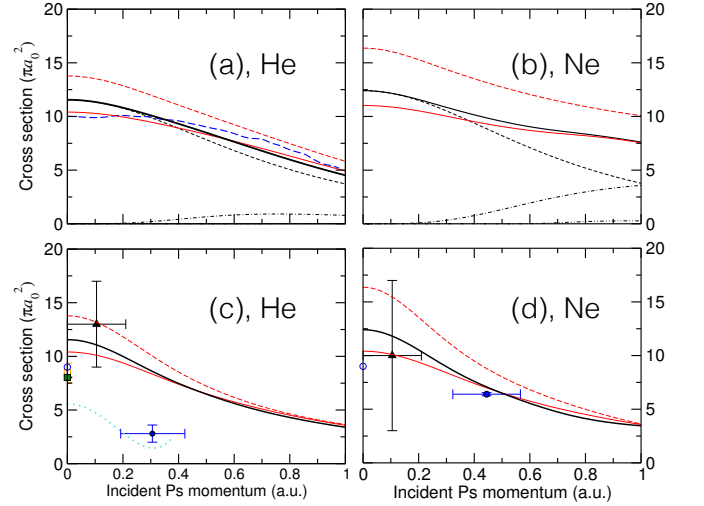


FIG. 5. Elastic-scattering cross sections for Ps on He (a) and Ne (b): total cross section calculated using MBT (thick solid line), with  $S$ - (dashed black line),  $P$ - (dot-dashed black line), and  $D$ -wave (dot-dot-dashed black line) partial contributions; FT (dashed red line) and FT+vdW (thin solid red line) calculations of Ref. [10]. Also shown for He is the 9-Ps-9-He-state calculation of Walters *et al.* [13] (thick dashed blue line). Momentum-transfer cross sections for Ps on He (c) and Ne (d) use the same symbols as in (a) and (b). Also shown are the experimental results of Canter *et al.* [38] (open square); Rytola *et al.* [39] (filled square); Coleman *et al.* [40] (open circle); Skalsey *et al.* [41] (filled circle); Nagashima *et al.* [42] (triangle); and Engbrecht *et al.* [43] (dotted turquoise line).

[13]. It is  $\sim 10\%$  smaller than the frozen-target (FT) calculation (1.86 a.u. [10]), highlighting the importance of including distortion of the target. For Ne, our scattering length of 1.76 a.u. is  $\sim 15\%$  smaller than the FT value (2.02 a.u.) but close to the FT+vdW result (1.66 a.u. [10]). The relatively small effect of the correlations, seen as the difference between the MBT and FT calculations, is due to cancellation of the positron- and electron-atom attraction ( $\hat{\Sigma}_E^\pm$ ) and the effect of screening  $\delta V_E$ .

The momentum-transfer cross sections are shown in Fig. 5 (c) and (d). Again, the present MBT calculation gives results that are similar to the FT+vdW calculation [10], especially for  $K \gtrsim 0.5$  a.u. For He, our calculation lies within the error bars of the experimental result of Nagashima *et al.* [42] but is  $\sim 30$ – $45\%$  larger than that of Canter *et al.* [38], Rytola *et al.* [39], and Coleman *et al.* [40]. The measurements of Skalsey *et al.* [41] and Engbrecht *et al.* [43] give much lower values. For Ne, there is agreement with the results of Skalsey *et al.* [41] and Nagashima *et al.* [42] but a  $\sim 40\%$  discrepancy with that of Coleman *et al.* [40]. Given the momentum-dependence of the calculated cross sections, the experimental data for Ne displays a greater degree of consistency than for He.

*Calculation of pickoff annihilation rates  $^1Z_{\text{eff}}$ .*—As a second application, we investigate the pickoff annihilation rate  $\lambda$ . It is parametrized as  $\lambda = 4\pi r_0^2 c n ^1Z_{\text{eff}}$ , where  $r_0$  is the classical electron radius,  $c$  is the speed of light,  $n$  is the number density of the gas, and the dimensionless quantity  $^1Z_{\text{eff}}$  gives the effective

TABLE I. Pickoff annihilation rates  ${}^1Z_{\text{eff}}$  for He and Ne at  $K = 0$ : best previous theory [8]; using frozen-target Ps wave function from Ref. [10]; present many-body theory in zeroth-order annihilation vertex (MBT); present many-body theory with vertex enhancement (MBT-VE); and experiment [11].

Atom	Prev. theory [8]	FT [10]	MBT	MBT-VE	Exp. [11]
He	0.0378	0.0273	0.0411	0.131	0.125
Ne	0.0922	0.0512	0.0932	0.255	0.235

number of target electrons available for pickoff annihilation. Our interest is in the value of  ${}^1Z_{\text{eff}}$  at small momenta, where only the  $S$ -wave contribution is nonzero. If the annihilation vertex is described in the zeroth-order (independent-particle) approximation, one has

$${}^1Z_{\text{eff}} = \frac{1}{4} \sum_{n\ell} \iint |\Psi_{0^+}(\mathbf{r}_e, \mathbf{r}_p)|^2 |\varphi_{n\ell}(\mathbf{r}_p)|^2 d\mathbf{r}_e d\mathbf{r}_p, \quad (6)$$

where  $\varphi_{n\ell}$  is the wave function of orbital  $n\ell$  in the ground-state atom, with  $\Psi_{0^+}$  such that the Ps center-of-mass motion is normalized to a plane wave at large distances from the atom. Previous calculations in this approximation for He [2–8, 10] and Ne [8, 10] yielded values of  ${}^1Z_{\text{eff}}$  that underestimated experimental data by a factor of 3 or more (see Table I). All of these calculations neglected the effect of short-range electron-positron correlations, which are known to enhance the annihilation rates by as much as a factor 2–5 [16, 45].

We take account of the correlation corrections in  ${}^1Z_{\text{eff}}$  by augmenting Eq. (6) with orbital-specific annihilation-vertex *enhancement factors*, which were calculated in Refs. [16, 45]. Specifically, we perform calculations for the lowest-energy  $J^{\Pi} = 0^+$  eigenstate for  $R_c = 10, 12, 14,$  and  $16$  a.u., giving values of  ${}^1Z_{\text{eff}}$  for four different  $K$ . These values depend on the maximum numbers of partial waves  $\ell_{\text{max}}$  and radial states per partial wave  $n_{\text{max}}$  included in Eq. (4). We extrapolate in  $\ell_{\text{max}}$  as  ${}^1Z_{\text{eff}}(\ell_{\text{max}}, n_{\text{max}}) = {}^1Z_{\text{eff}}(\infty, n_{\text{max}}) + A(\ell_{\text{max}} + 1/2)^{-2}$  and subsequently in  $n_{\text{max}}$  as  ${}^1Z_{\text{eff}}(\infty, n_{\text{max}}) = {}^1Z_{\text{eff}} + \alpha n_{\text{max}}^{\beta}$ , where we typically find  $\beta \approx -4$  [46]. The Ps wave function is normalized to the center-of-mass plane wave by calculating the center-of-mass density away from the atom and cavity wall and comparing it with  $\sin^2(KR + \delta_0)/K^2R^2$  (see Ref. [47] for details). Finally, we fit the four values to the effective-range form  ${}^1Z_{\text{eff}}(K) \simeq {}^1Z_{\text{eff}}(0) + CK^2$  [48] to deduce  ${}^1Z_{\text{eff}}(0)$ . The results are shown in Table I. Neglecting the enhancement factors, we find good agreement with the previous best zeroth-order vertex results. Including the vertex enhancement produces near-perfect agreement with experimental values for room-temperature Ps.

*Summary.*—The MBT of Ps interactions with atoms was presented and applied to calculate scattering cross sections and pickoff annihilation rates in He and Ne. The calculations show that the net effect of the dispersion interaction (electron and positron polarization of the atom and screening of the electron-positron Coulomb interaction by atomic electrons) is

relatively small, and close to that described by the van der Waals interaction with a short-range cutoff. The MBT gives pickoff annihilation rates in excellent agreement with experiment.

*Acknowledgments.*—DGG was supported by the EPSRC UK, grant EP/N007948/1. ARS was supported by the Department for Employment and Learning, Northern Ireland, UK.

\* Correspondences to: [d.green@qub.ac.uk](mailto:d.green@qub.ac.uk)

† [aswann02@qub.ac.uk](mailto:aswann02@qub.ac.uk)

‡ [g.gribakin@qub.ac.uk](mailto:g.gribakin@qub.ac.uk)

- [1] S. J. Brawley, S. E. Fayer, M. Shipman, and G. Laricchia, *Phys. Rev. Lett.* **115**, 223201 (2015).
- [2] P. A. Fraser and M. Kraidy, *Proc. Phys. Soc.* **89**, 533 (1966).
- [3] P. A. Fraser, *J. Phys. B* **1**, 1006 (1968).
- [4] M. I. Barker and B. H. Bransden, *J. Phys. B* **1**, 1109 (1968).
- [5] M. I. Barker and B. H. Bransden, *J. Phys. B* **2**, 730 (1969).
- [6] R. J. Drachman and S. K. Houston, *J. Phys. B* **3**, 1657 (1970).
- [7] P. K. Biswas and S. K. Adhikari, *Chem. Phys. Lett.* **317**, 129 (2000).
- [8] J. Mitroy and I. A. Ivanov, *Phys. Rev. A* **65**, 012509 (2001).
- [9] J. Mitroy and M. W. J. Bromley, *Phys. Rev. A* **67**, 034502 (2003).
- [10] A. R. Swann and G. F. Gribakin, “Positronium scattering by noble-gas atoms using a spherical cavity,” *To be submitted to Phys. Rev. A* (2017).
- [11] M. Charlton, *Rep. Prog. Phys.* **48**, 737 (1985).
- [12] H. Saito and T. Hyodo, *Phys. Rev. Lett.* **97**, 253402 (2006).
- [13] H. Walters, A. Yu, S. Sahoo, and S. Gilmore, *Nucl. Instrum. and Meth. B* **221**, 149 (2004).
- [14] L. J. M. Dunlop and G. F. Gribakin, *J. Phys. B* **39**, 1647 (2006).
- [15] D. G. Green, J. A. Ludlow, and G. F. Gribakin, *Phys. Rev. A* **90**, 032712 (2014).
- [16] D. G. Green and G. F. Gribakin, *Phys. Rev. Lett.* **114**, 093201 (2015).
- [17] H. P. Kelly, *Phys. Rev.* **131**, 684 (1963).
- [18] H. P. Kelly, *Phys. Rev.* **136**, B896 (1964).
- [19] H. P. Kelly, *Phys. Rev.* **160**, 44 (1967).
- [20] Y. Cheng, L. Y. Tang, J. Mitroy, and M. S. Safronova, *Phys. Rev. A* **89**, 012701 (2014).
- [21] M. Amusia, N. Cherepkov, L. Chernysheva, and S. Shapiro, *Phys. Lett. A* **46**, 387 (1974).
- [22] M. Amusia, N. Cherepkov, A. Tancic, S. G. Shapiro, and L. Chernysheva, *J. Exp. Theor. Phys.* **68**, 2023 (1975).
- [23] M. Y. Amusia, N. A. Cherepkov, L. V. Chernysheva, D. M. Davidović, and V. Radojević, *Phys. Rev. A* **25**, 219 (1982).
- [24] M. Y. Amusia, N. A. Cherepkov, L. V. Chernysheva, and S. G. Shapiro, *J. Phys. B* **9**, L531 (1976).
- [25] V. A. Dzuba, V. V. Flambaum, W. A. King, B. N. Miller, and O. P. Sushkov, *Phys. Scripta* **T46**, 248 (1993).
- [26] G. F. Gribakin and J. Ludlow, *Phys. Rev. A* **70**, 032720 (2004).
- [27] D. G. Green, “Positron cooling and annihilation in noble gases,” ([arXiv:1706.01434](https://arxiv.org/abs/1706.01434)).
- [28] D. G. Green, “Probing positron cooling in noble gases via annihilation  $\gamma$  spectra,” ([arxiv.org/abs/1706.04948](https://arxiv.org/abs/1706.04948)).
- [29] A. A. Abrikosov, L. P. Gorkov, and I. E. Dzyaloshinski, *Methods of Quantum Field Theory in Statistical Physics* (Dover, New York, 1975).
- [30] W. H. Dickhoff and D. V. Neck, *Many body theory exposed! - Propagator Description of Quantum Mechanics in Many-Body*

*Systems - 2nd ed.* (World Scientific, Singapore, 2008).

- [31]  $\mathcal{Q}_E^\pm$  acts as  $\mathcal{Q}_E^\pm \psi_\varepsilon(\mathbf{r}) = \int \Sigma_E^\pm(\mathbf{r}, \mathbf{r}') \psi_\varepsilon(\mathbf{r}') d\mathbf{r}'$ .
- [32] W. R. Johnson and C. Guet, *Phys. Rev. A* **49**, 1041 (1994).
- [33] See Ref. [20] for higher-order calculations.
- [34] V. A. Dzuba and G. F. Gribakin, *Phys. Rev. A* **49**, 2483 (1994).
- [35]  $S_{0\ell}^\pm > 1$  is a necessary condition to support a positron or (extra) electron bound state [34].
- [36] R. Brown, Q. Prigent, A. R. Swann, and G. F. Gribakin, *Phys. Rev. A* **95**, 032705 (2017).
- [37] This ensures that the Dyson states used in Eq. (4) form orthonormal bases.
- [38] K. F. Canter, J. D. McNutt, and L. O. Roellig, *Phys. Rev. A* **12**, 375 (1975).
- [39] K. Rytsoala, J. Vettenranta, and P. Hautojarvi, *J. Phys. B* **17**, 3359 (1984).
- [40] P. G. Coleman, S. Rayner, F. M. Jacobsen, M. Charlton, and R. N. West, *J. Phys. B* **27**, 981 (1994).
- [41] M. Skalsey, J. J. Engbrecht, C. M. Nakamura, R. S. Vallery, and D. W. Gidley, *Phys. Rev. A* **67**, 022504 (2003).
- [42] Y. Nagashima, T. Hyodo, K. Fujiwara, and A. Ichimura, in *The International Conference on the Physics of Electronic and Atomic Collisions, Vancouver, 1995, Abstracts of Contributed Papers* (1995).
- [43] J. J. Engbrecht, M. J. Erickson, C. P. Johnson, A. J. Kolan, A. E. Legard, S. P. Lund, M. J. Nyflot, and J. D. Paulsen, *Phys. Rev. A* **77**, 012711 (2008).
- [44] At low momenta, the FT+vdW calculation is sensitive to the choice of cutoff radius in the model van der Waals potential.
- [45] D. G. Green and G. F. Gribakin, [arXiv:1703.06980](https://arxiv.org/abs/1703.06980), To appear in *Prog. Theor. Chem. Phys.* (2017).
- [46] Extrapolation in  $\ell_{\max}$  typically reduces the value of  $^1Z_{\text{eff}}$  by  $\sim 20\%$ , while extrapolation in  $n_{\max}$  is much less important, changing  $^1Z_{\text{eff}}$  by  $\lesssim 1\%$ .
- [47] A. R. Swann, D. G. Green, and G. F. Gribakin, "Positronium scattering and annihilation in noble gases," To be submitted to *Phys. Rev. A* (2017).
- [48] J. Mitroy, *Phys. Rev. A* **66**, 022716 (2002).